IEEE Access
Multidisciplinary | Rapid Review | Open Access Journal

Received 18 October 2022, accepted 15 November 2022, date of publication 17 November 2022,
date of current version 23 November 2022.

Digital Object Identifier 10.1109/ACCESS.2022.3223126

RESEARCH ARTICLE

Five-Level Hysteresis DTC of Open-End Winding Permanent Magnet Synchronous Motors With Zero-Sequence Currents Suppression and Torque Ripple Reduction

YULEI YANG, QIAN WANG, (Member, IEEE), AND JING SHANG
Electrical Engineering Department, Harbin Institute of Technology, Harbin 150001, China

Corresponding author: Qian Wang (q.wang@hit.edu.cn)

This work was supported by the Natural Science Foundation of China (NSFC) under Grant 52277039.

ABSTRACT Direct torque control (DTC) systems for open-end winding permanent magnet synchronous motors (OEW-PMSM) with common DC bus generate zero sequence currents (ZSC) and large torque ripple, resulting in increased system loss and poor operating characteristics. In this paper, a DTC based on five level torque hysteresis (FLTH) is proposed to improve the system performance. Firstly, an online calculation and selection strategy based on switch table is designed to suppress ZSC. By analyzing the composition of zero sequence voltage and using the double vector method to suppress it, the ZSC can totally be suppressed in theory, without affecting the system performance. On this basis, this paper proposes to add FLTH to DTC to reduce torque ripple. FLTH can not only effectively use many voltage vectors, but also reduce torque ripple. In the case study, the torque ripple rate has been reduced by 53%. Through simulation and experiment, the conventional DTC and the FLTH DTC are compared, and the results prove the validity of the proposed strategy.

INDEX TERMS Direct torque control (DTC), open-end winding permanent magnet synchronous motor (OEW-PMSM), five-level torque hysteresis (FLTH), zero-sequence current (ZSC), torque ripple.

I. INTRODUCTION

As a special type of permanent magnet synchronous motor (PMSM), the open-end winding PMSM (OEW-PMSM) has attracted increased attentions in recent years, particularly in the transportation sector (such as electric vehicles) where speed regulation performance is essentially crucial [1], [2], [3]. Because of its unique structure, the OEW-PMSM can improve the voltage utilization ratio, and expand the speed range. For an OEW-PMSM, it is usually driven by dual inverters with common DC bus using direct torque control strategy, and the system enjoys the features of low cost, flexible control, fast response, etc [4], [5]. Theoretically speaking, a dual-inverter fed OEW-PMSM can achieve twice the speed range of a PMSM. However, the system suffers from one major drawback, which is the ZSC. The ZSC will increase the busbar current [6], thereby increasing the loss of power devices and affecting the operating characteristics of the motor.

Dual inverters are connected to the same DC source through a common DC bus, which does not require high equipment, but forms a zero-sequence voltage in the inverter circuit [7]. ZSC will not only reduce the utilization rate of the inverter, but also cause the ripple of torque and flux linkage, which affects the promotion and application of dual-inverter fed OEW-PMSM with common DC bus [8], [9]. Therefore, suppression of ZSC has become a hot issue. For the ZSC suppression method of the dual-inverter structure, software suppression methods are more commonly used. In addition, the dual-inverter system has more redundant switching states, which provides conditions for suppressing the ZSC through modulation. The dual-inverter structure will

The associate editor coordinating the review of this manuscript and approving it for publication was Atif Iqbal.

generate 19 switching vectors, some of which do not generate common-mode voltage.

In [10], only 7 vectors that do not generate zero sequence voltage are used for PWM method. Although the zero-sequence voltage is eliminated, it reduces the utilization rate of the DC bus voltage. Reference [11] designs a software program to clamp and fix the switching state of one inverter, while the other inverter acts as a compensator to modulate the desired voltage. And the working time of the zero vector is reasonably arranged in the corresponding position in the switching cycle, the positive and negative values of the common mode voltage in one MOSFET working cycle can cancel each other, the average value is zero, and the purpose of reducing the switching frequency can be achieved. But under this method, the common mode voltage will change with the operating frequency. The high-frequency variation of the common mode voltage will induce shaft voltage and shaft current on the motor shaft, which is also harmful to the operation of the motor. In addition, although 19 voltage vectors are used in this method, there is still the problem of low DC bus voltage utilization.

Similarly, the article [12], [13], [14] studied the influence of the zero-sequence voltage generated by the zero vector on the common mode voltage of the inverter. By designing and calculating the position and time of the zero vector in a switching cycle, it can be realized to eliminate common mode voltage.

As a new type of motor structure, the dual-inverter OEW-PMSM provides more voltage vectors, which provides the conditions for the improvement of the performance of the DTC. But the DTC has the problem of large torque ripple. In view of the drawbacks of the conventional DTC algorithm, many efforts have been made in literature to improve the control performance of DTC. The main solutions can be divided into three types: changing the switch table or torque hysteresis adjustment; adding SPWM to the DTC strategy and model predictive control (MPC) combined with torque control [15], [16], [17], [18], [19], [20], [21], [22], [23].

The first control strategy to change the switch table or torque hysteresis regulation is mainly achieved by designing a complicated hysteresis regulator or increasing the number of the voltage vectors [15], [16], [17]. In the second method, the space pulse modulation (SVM) is added to the DTC strategy, which is mainly through the integration of vector control and DTC [18], [19], [20]. In the third solution, model prediction combined with torque control is used to calculate the most appropriate voltage vector through predictive control algorithm, thus eliminating the design of switch table [21], [22], [23].

This paper proposes a direct torque control strategy for OEW-PMSM systems with common DC bus based on five-level hysteresis. This strategy not only suppresses the ZSC, but also realizes the effective suppression of torque ripple. The rest of the paper will proceed in accordance with the following aspects. In Section II, the mathematical model and voltage dual-inverter model with common DC sources fed OEW-PMSM are established. In Section III, the control algorithm of five-level hysteresis DTC for common DC bus OEW-PMSM is proposed. In Section IV, losses and torque ripple of the algorithm are analyzed. In Section V, through experiment results, the rationality and correctness of the proposed strategy are proved. Finally, the conclusion is given in Section VI.

II. MATHEMATICAL MODEL OF OEW-PMSM WITH COMMON DC BUS

The block diagram of standard OEW-PMSM with common DC bus is presented in Fig. 1. Since the neutral point of the three-phase permanent magnet synchronous motor is open, the common DC bus structure provides a loop for the harmonic current, and the harmonic current also constitutes a part of the ZSC, so the third harmonic of the OEW-PMSM cannot be ignored. The representation of the stator flux linkage in the ABC coordinate system is as follows:

$$\begin{bmatrix} \psi_{sA} \\ \psi_{sB} \\ \psi_{sC} \end{bmatrix} = \begin{bmatrix} L_A & M_{AB} & M_{AC} \\ M_{BA} & L_B & M_{BC} \\ M_{CA} & M_{CB} & L_C \end{bmatrix} \begin{bmatrix} i_{sA} \\ i_{sB} \\ i_{sC} \end{bmatrix} + \begin{bmatrix} \psi_{rA} \\ \psi_{rB} \\ \psi_{rC} \end{bmatrix} \tag{1}$$

where

$$\begin{bmatrix} \psi_{rA} \\ \psi_{rB} \\ \psi_{rC} \end{bmatrix} = \psi_{1r} \begin{bmatrix} \cos\theta_r \\ \cos(\theta_r - 2\pi/3) \\ \cos(\theta_r + 2\pi/3) \end{bmatrix} + \psi_{3r} \begin{bmatrix} \cos 3\theta_r \\ \cos 3\theta_r \\ \cos 3\theta_r \end{bmatrix} \tag{2}$$

The angle between α − axis and d − axis is the rotor electrical angular $\theta_r$as showed in Fig. 2, $L_i(i = A, B, C)$ are self-inductance of each phase windings, $M_{ij}(i, j = A, B, C; i \neq j)$ are mutual inductance every two phase stator windings, ψ_{1r}, ψ_{3r} are fundamental and third harmonic component of rotator permanent flux, respectively.

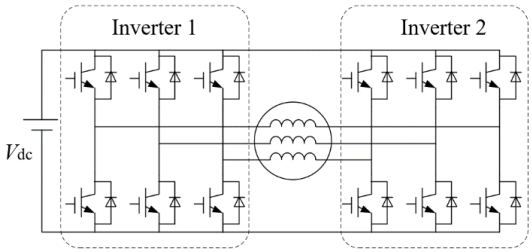

FIGURE 1. Dual-inverter fed OEW-PMSM with common dc bus topology.

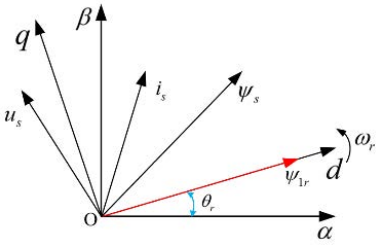

FIGURE 2. Definitions of the fundamental component coordinate system.

In the ABC coordinate system, the three-phase stator voltage is as follows:

$$\begin{bmatrix} u_{sA} \\ u_{sB} \\ u_{sC} \end{bmatrix} = \begin{bmatrix} R_s & 0 & 0 \\ 0 & R_s & 0 \\ 0 & 0 & R_s \end{bmatrix} \begin{bmatrix} i_{sA} \\ i_{sB} \\ i_{sC} \end{bmatrix} + \frac{d}{dt} \begin{bmatrix} \psi_{sA} \\ \psi_{sB} \\ \psi_{sC} \end{bmatrix} \tag{3}$$

where R_s is phase resistance.

In the $dq0$ coordinate system, the electromagnetic torque can be further simplified as follows:

$$T_e = \frac{3}{2} p_n \left[\psi_{1r} i_{sq} + (L_d - L_q) i_{sq} i_{sd} - 3\sqrt{3} \psi_{3r} \sin(3\theta_r) i_{s0} \right] \tag{4}$$

where p_n is number of pole pairs, i_{sq}, i_{sd} are the current of q-axis and d-axis in the $dq0$ coordinate system, i_{s0} is the zero sequence current of the stator winding, and the inductances of the d-axis and q-axis are L_d, L_q, respectively.

According to equation (4), the electromagnetic torque of three-phase OEW-PMSM includes main electromagnetic torque, reluctance torque and harmonic zero-sequence torque. The reluctance of the motor studied in this paper is zero and is not considered. If the ZSC is not zero, on the one hand, it will affect the torque output, on the other hand, it will increase the system loss and reduce the maximum output power. In addition, the stability of the system will also be affected. Therefore, to reduce torque ripple, it is first necessary to suppress ZSC.

In this paper, DTC is applied to OEW-PMSM with common DC bus. Applying the characteristics of multiple voltage vectors of OEW-PMSM with dual inverters, designing a switch table for online calculation, making full use of different voltage vectors to output the electromagnetic torque of the motor. The ZSV and the third harmonic of the back EMF are calculated online and suppressed in each electric cycle.

OEW-PMSM is driven and powered by two parallel inverters composed of 12 switches. The switching state of power switches on the three-phase 3H bridge arm determines the working state of the two parallel inverters. For each inverter module, as shown in Fig. 3, their voltage vector spatial distribution is the same as the conventional three-phase two-level inverter.

The combination of these voltages can generate 19 voltage vectors. As shown in Fig. 4, the system has 19 voltage space vectors, namely 18 non-zero voltage vectors and 1 zero vector on $\alpha\beta$ plane. Moreover, for the same voltage vector, it may correspond to several different state combinations. For example, the six switch states corresponding to u_5 can be expressed as: $\{43', 57', 58', 61', 72', 82'\}$. In the case of voltage vector $43'$, Inverter 1 generates the voltage vector 4 (011). Meanwhile, Inverter 2 generates the voltage vector $3'$ (010).

III. PROPOSED MODULATION STRATEGY BASED ON FLTH CONTROLLER OF OEW-PMSM

A. ZSC SUPPRESSION METHOD BASED ON ONLINE CALCULATION OF SWITCH TABLE

The ZSC mainly caused by the ZSV generated by the two inverters with common DC bus and the third harmonic of the back EMF. The equivalent zero sequence circuit is shown in Fig. 5. ZSV can be expressed as follows:

$$\begin{aligned} u_{s0} &= R_s i_{s0} + L_{s\sigma 1} \frac{d}{dx} i_{s0} - 3\psi_{3r}\omega_r \sin(3\theta_r) \\ &= u_{s01} - u_{s02} - e_3 \end{aligned} \tag{5}$$

where i_{s0} is the stator ZSC, $L_{s\sigma 1}$ is phase leakage inductance, ω_r is the electrical angular velocity of the rotor and e_3 is the third harmonic of the back EMF.

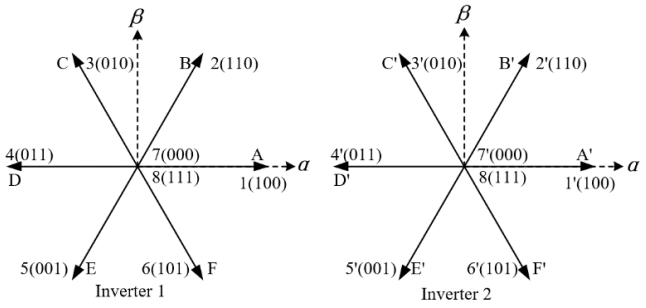

FIGURE 3. Single inverter vector.

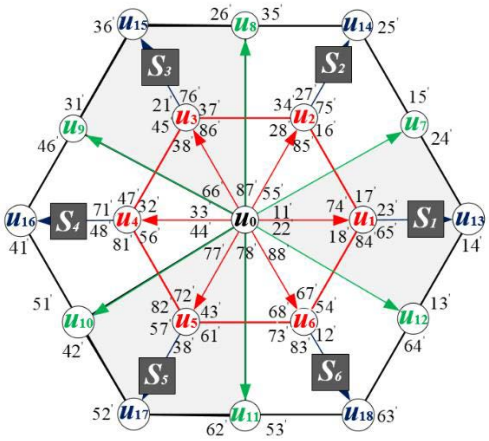

FIGURE 4. 19 Voltage vectors.

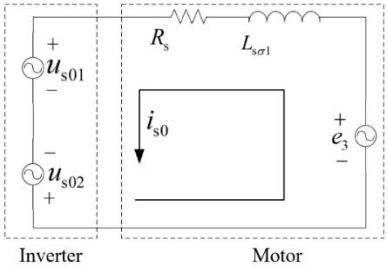

FIGURE 5. Equivalent zero sequence circuit.

According to (5), the ZSV can be directly obtained by simply calculating the common mode voltage generated by

the two inverters. In the DTC, the switch table has been designed, then the switch state of the inverter can be determined. Through the analysis of the voltage vector switch state, we can directly obtain the common mode voltage. In the $\alpha\beta 0$ coordinate system, the common mode voltage can be directly determined after the switch state is determined. For example, the common mode voltages corresponding to the 6 switch states of u_5 are shown in Table 1. In the process of designing the switch table, we only select one switch state of u_5, then the corresponding common mode voltage can be known. Assuming that u_5 is selected as the active vector in a working cycle, and the corresponding common mode voltage is $1/3V_{dc}$, then the ZSV can be known as follows:

$$u_{s0} = \frac{1}{3}V_{dc} - e_3 \tag{6}$$

where V_{dc} is bus voltage.

TABLE 1. The common mode voltages corresponding to the 6 switch states of u_5.

switch states	43' (011010)	57' (001000)	58' (001111)	61' (101100)	72' (000110)	82' (111110)
u_{cmv}	$1/3V_{dc}$	$1/3V_{dc}$	$-2/3V_{dc}$	$1/3V_{dc}$	$-2/3V_{dc}$	$1/3V_{dc}$

After determining the ZSV, the next step is to suppress the ZSC. In this paper, zero vector is used to modulate the ZSV. There are 10 switching states for the zero vector of dual inverters common DC bus three-phase OEW-PMSM. In this paper, the zero vectors 78' (000111) and 87' (111000) are selected, and the zero vector in the opposite direction is selected according to the direction of the ZSV in the circuit. Moreover, the other 8 zero-vectors will not generate ZSV in the actual control process, that is, they cannot play a role in suppressing the ZSC. In a charge balance in an electrical cycle, we can get the equation as follows:

$$\begin{cases} T_s = T_1 + T_2 \\ e_3 = T_1 u_{cmv} + T_2 u_0 \end{cases} \tag{7}$$

where u_{cmv} is common mode voltage of active vector, u_0 is voltage of zero vector, T_s is an electrical cycle, and T_1, T_2 are the working hours of active vector and zero vector respectively.

After simplification, it can be obtained, if $u_{cmv} = -1/3V_{dc}$, the result is shown in (8), and if $u_{cmv} = 1/3V_{dc}$, the result is shown in (9).

$$\begin{cases} T_1 = \frac{1}{4}T_s - \frac{3}{4}\frac{e_3}{V_{dc}}T_s \\ T_2 = \frac{3}{4}T_s + \frac{3}{4}\frac{e_3}{V_{dc}}T_s \end{cases} \tag{8}$$

$$\begin{cases} T_1 = \frac{1}{4}T_s + \frac{3}{4}\frac{e_3}{V_{dc}}T_s \\ T_2 = \frac{3}{4}T_s - \frac{3}{4}\frac{e_3}{V_{dc}}T_s \end{cases} \tag{9}$$

B. PROPOSED DTC STRATEGY BASED ON FLTH

From Fig. 4 of the distribution of the voltage vector on the fundamental plane, we can see that in the same direction of each large vector, there is a small vector, such as vectors u_1 and u_{13}. These two vectors have the following characteristics: the two vectors have the same increase or decrease effect on the torque or flux linkage, that is, increase or decrease the torque or flux linkage at the same time; the difference is that the greater the vector amplitude, the opposite rotation the increment of moment or flux linkage is also larger.

In order to reduce torque ripple and take full advantage of the more abundant voltage vectors of OEW-PMSM, the third-level torque hysteresis comparator in equation is changed to the following five-level hysteresis comparator:

$$\tau = \begin{cases} +2 & T_e^* - T_e > B_h \\ +1 & B_h > T_e^* - T > B_l \\ 0 & other \\ -1 & -B_l > T_e^* - T > -B_h \\ -2 & -B_h > T_e^* - T \end{cases} \tag{10}$$

where B_h, B_l is the bandwidth of the outer layer and inner layer of the FLTH controller in sequence. The principle of the FLTH controller is shown in Fig. 6. A five-level hysteresis is added to the three-level hysteresis. If the large vector acting at the k^{th} moment is replaced by a voltage vector with a smaller amplitude in the same direction, the torque will decrease in a Ts period. A small amount will become smaller, and the instantaneous sampled torque value at k+1 at the end of the control period can be kept within the set inner hysteresis bandwidth. At the next moment k+1, since the actual value is still within the given value range, a small vector is also used. When the actual torque value exceeds the inner hysteresis bandwidth at k+3, but does not exceed the outer hysteresis bandwidth, a small vector is used to reduce the torque, so that it can be restored to a small torque ripple interval, so as to achieve the purpose of reducing torque ripple.

This article mainly studies the suppression strategy of torque ripple, so the flux linkage controller still uses the conventional two-level hysteresis controller. Since the switch status of the lower arm is opposite to that of the upper arm, only the switch status of the upper bridge arm is listed here, and the switch table based on the FLTH controller DTC can be obtained as shown in Table 2. In this paper, 12 certain switch states are selected in six sectors to design the switch table, where the common mode voltage generated by all the switch states is $1/3V_{dc}$, but there are different voltage directions.

The size of the hysteresis width determines the type of vector that acts on the next control cycle, and has a decisive effect on the performance of the control system torque. In this paper, we set the outer bandwidth of the five-level hysteresis loop to the same width as the conventional three-level hysteresis loop. Although the large vector is twice as large as the small vector, considering the sector width, the different positions of the vector function leave a certain margin. I conducted a detailed simulation analysis on the relationship between the

width of the two-stage hysteresis loop and compared it with the experiment. The results of the analysis curve are shown in Figure 7. The results show that the ratio of the width of the two-stage hysteresis loop has a significant impact on the torque ripple, and the optimal result is finally selected for the experiment. The DTC block diagram based on the FLTH is shown in Fig.8. The program flowchart of the proposed FLTH strategy is shown in Fig. 9.

TABLE 2. Vectors switching table of FLTH controller based DTC.

φ	τ	S_1	S_2	S_3	S_4	S_5	S_6
	+2	25	36	41	52	63	14
	+1	16	21	32	43	12	23
1	0	77	77	77	77	77	77
	-1	12	23	16	21	32	43
	-2	63	14	25	36	41	52
	+2	36	41	52	63	14	25
	+1	21	32	43	12	23	16
-1	0	77	77	77	77	77	77
	-1	23	16	21	32	43	12
	-2	14	25	36	41	52	63

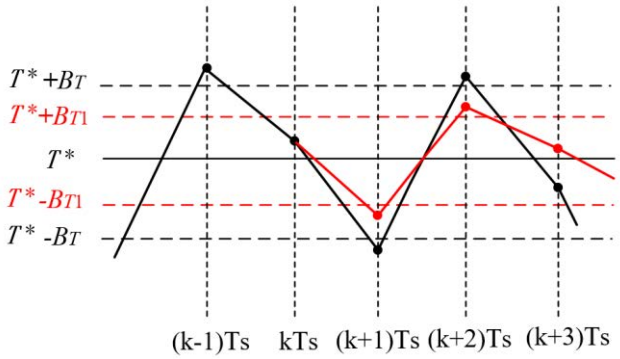

FIGURE 6. Principle of the five-level torque hysteresis controller.

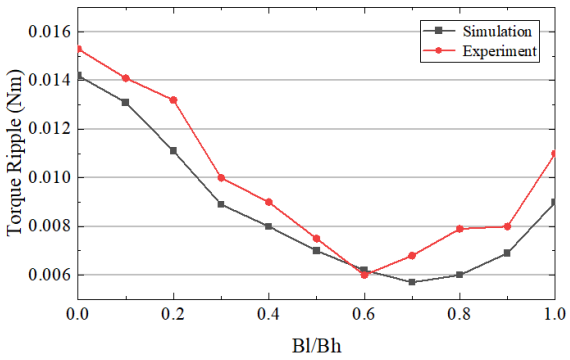

FIGURE 7. Relationship between Bl/Bh and torque ripple.

The detailed implementation process of the proposed strategy is as follows.

Step 1: The voltage vector plane is divided into six sectors, and the specific division result is shown in Fig. 4.

Step 2: Calculate the phase angle of the voltage and determine which sector is in $S_i(i = 1\text{-}6)$.

Step 3: Select the voltage vector in the switch table according to the output signal of the five-level torque hysteresis and flux hysteresis.

Step 4: Determine the direction and magnitude of the common mode voltage, and select the zero vector opposite to the direction

Step 5: Use the online calculation switch table to calculate the working time T_1 and T_2 of the active vector and the zero vector.

Step 6: Output the corresponding voltage vector signal according to the calculated T_1 and T_2.

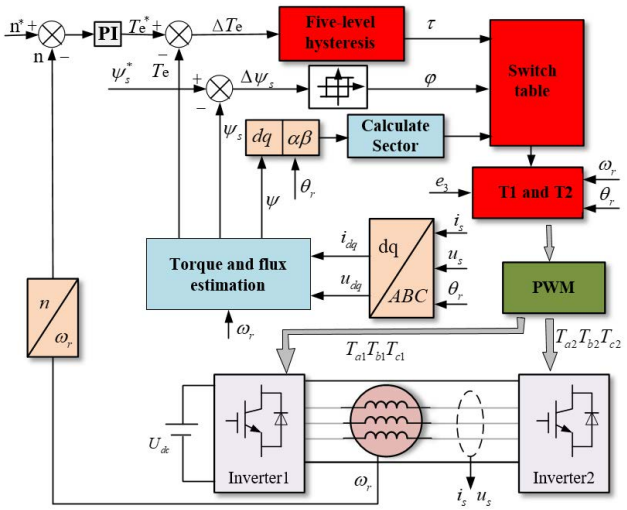

FIGURE 8. The DTC block diagram based on the five-level torque hysteresis.

IV. LOSS ANALYSIS AND TORQUE RIPPLE CHARACTERISTIC

The impact of the proposed method on motor performance, including power loss and torque ripple, needs to be investigated, as described in this section. The motor parameters used in the simulation and experiment are shown in Table 3.

TABLE 3. Nominal parameters of an OEW-PMSM drive.

Symbols	Parameters	Values	Units
P_{rated}	Rated power	750	W
p_n	Number of poles	4	-
R_S	Stator resistance	1.4	Ω
L_d	d-axis inductance	2.96	mH
L_q	q-axis inductance	2.96	mH
ψ_{1r}	Rotor flux linkage	0.117223	Wb
ψ_{3r}	Third harmonic flux linkage	0.003	Wb
N_M	Test maximum speed	400	rpm
T_M	Test maximum torque	1	Nm

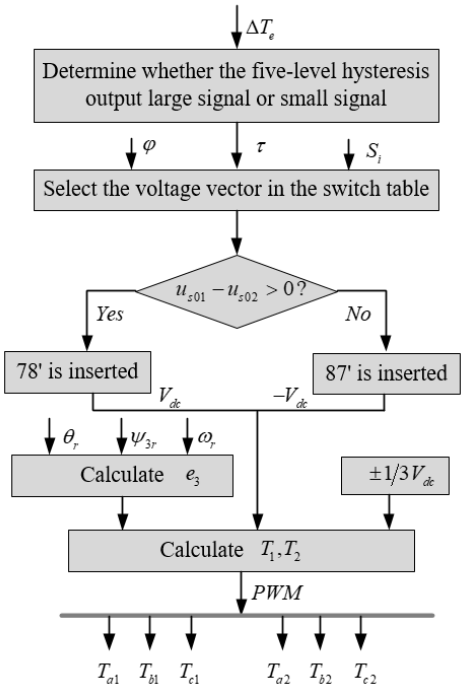

FIGURE 9. The program flowchart.

A. LOSS ANALYSIS

Currents with imperfect waveforms cause additional power losses in the system. In addition to mechanical losses, the main power losses of OEW-PMSMs include copper and iron losses. Mechanical losses can be considered constant. For the copper loss, ignoring the skin effect, for the harmonic components contained in the phase current, the average copper loss can be calculated by (11)

$$P_{copper} = \frac{3\omega}{2\pi}\int_0^{2\pi/\omega} i^2 R dt \tag{11}$$

Without suppression, the magnitude of steady-state ZSC will be very large, which will seriously affect the phase currents and cause relatively large energy loss. After the suppression, the ZSC is zero, which directly avoids the power loss of this part. Hence, the phase currents before and after ZSC suppression are shown in Fig. 10, and the copper losses of the motor are 8.4W and 0.525W respectively. It can be seen that the copper loss of the motor without suppressing the ZSC is 16 times that after the suppression.

Considering that the switching frequency will increase the loss, the switching frequencies of the three methods are analyzed, and the results are shown in the Fig. 11. We can find that the switching frequency of the proposed method is indeed higher than that of the traditional DTC, and fluctuates in a certain range with the speed change. This is because the proposed method increases the zero vector in the process of suppressing the ZSC. At the same time, the process of reducing torque ripple is accompanied by the problem of selecting the optimal vector. This inevitably increases the switching frequency.

B. TORQUE RIPPLE ANALYSIS

Fig. 12 shows the difference in torque ripple characteristics between the proposed method and the conventional method. The rotational speed is 400 rpm, and the load is set to 0.4 Nm. The quantitative comparison results of the two methods are shown in Table 4. It can be seen from the table that the torque ripple rate of the method proposed in this paper is 3.2%, while that of the traditional method is 6.9%, indicating that the algorithm strategy has obvious effects and can reduce the torque ripple rate. In addition, under the rated torque condition, the torque ripple of the motor remains stable with the speed change.

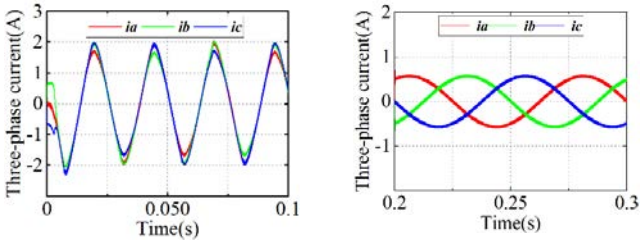

FIGURE 10. Stator three-phase current. (a) ZSC is not suppressed. (b) ZSC is suppressed.

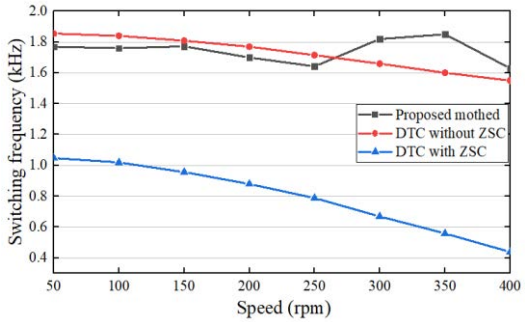

FIGURE 11. Switching frequencies comparison under different speeds.

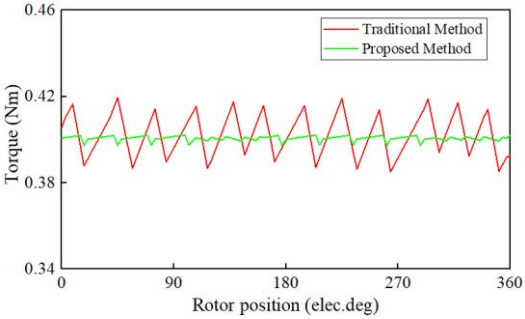

FIGURE 12. Torque ripple of the proposed method and the conventional method.

The resultant torque ripple consists of two parts from (4). The first is the torque ripple introduced by the q-axis current. Since the inductances of the d-axis and q-axis are equal in this paper, the second part is zero. The last one is the torque ripple introduced by the third harmonic flux linkage.

TABLE 4. Torque characteristics of proposed mothed and conventional mothed.

Mothed	Max torque (Nm)	Min torque (Nm)	Average torque (Nm)	Torque ripple (Nm)	Rate of ripple
Conventional mothed	0.4150	0.3876	0.4	0.0274	6.9%
Proposed mothed	0.4040	0.3913	0.4	0.0127	3.2%

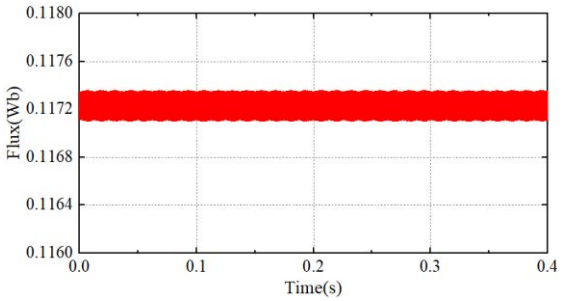

FIGURE 13. The rotor flux linkage.

The torque ripple introduced by the q-axis current against fundamental flux linkage is obtained as

$$T_1 = \frac{3}{2} p_n \psi_{1r} i_{sq} \tag{12}$$

where ψ_{1r} is shown in Fig. 13. The flux fluctuates around 0.1172Wb. The results of the proposed method are basically the same as those of conventional DTC.

V. EXPERIMENTAL VALIDATION

The experimental setup is shown in Figure 14. Two three-phase voltage source inverters are connected to the ends of each winding. The proposed algorithm is verified by using the driver of TI DSP28379d system and the 0.75 kW inner rotor OEW-PMSM, and the system parameters are shown in Table 3. The PWM switching frequency is 20 kHz, and the dead time is set to 2 μs. The DC bus voltage is 24 V.

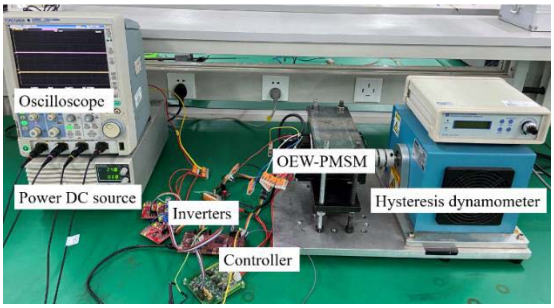

FIGURE 14. The experimental rig.

A. STEADY-STATE EXPERIMENTAL STUDY

To investigate the steady-state performance of the proposed system, DTC with ZSC, DTC with ZSC suppression, the proposed strategy and DRM-DTC in [10] are adopted in a three-phase OEW-PMSM, respectively. These three methods are defined as methods I, II III and IV respectively.

Figure 15-18 shows the steady-state operation of the four methods. Phase current, ZSC and torque are all verified at 400r/min. It can be seen that the ZSC of method I is obvious, because it is a DTC scheme for PMSM and does not consider suppressing the ZSC. The latter two methods suppress ZSC according to the operation characteristics of OEW-PMSM, and the motor runs stably. Through the fast Fourier transform (FFT) analysis of the phase currents, the total harmonic distortion (THD) and third harmonic component of the four methods are 58.53%, 14.20%, 11.36%, 12.20%, 58.65%, 8.21%, 6.13% and 6.15% respectively. Through the self comparison of the first three methods, it is found that the third method has better steady-state performance. At the same time, by comparing the method proposed in this paper with the method IV, it is found that although the two methods have two completely different directions, the experimental results are basically the same, which also proves the effectiveness of the algorithm in this paper. Although ZSC suppression measures were applied in the latter three methods, a small amount of ZSC could still be found in the current. The reasons are analyzed as follows. First, in order to ensure that the switch tube is not damaged, the dead time must be added to the PWM signal. The existence of dead time will introduce uncontrollable ZSV in the PWM duty cycle, resulting in the existence of a small amount of ZSC. Secondly, the experimental results are not as perfect as the simulated waveforms, also because the simulation modeling and experimental control strategy only consider the third harmonic, and the experimental motor will have higher harmonics, which also affects the experimental results to a certain extent.

From the steady-state torque waveforms of method I and method II, it can be seen that after suppressing ZSC, the torque ripple is reduced to a certain extent. This is because in (4), the third harmonic magnetic potential and the ZSC only constitute a very small part, and the ZSC is reduced to 0, which eliminates the influence of the third part on the torque ripple, thereby affecting the torque ripple. There is a certain reduction effect. But due to the shortcomings of the DTC algorithm itself, the torque ripple is still large. Then, after comparing Method II and Method III, it can be found that the torque ripple is significantly reduced. It shows that the method proposed in this paper can improve the steady-state performance of the motor and effectively reduce the torque ripple. But the final experimental effect still has a certain torque ripple, the reasons are as follows. The algorithm proposed in this paper is still carried out on the basis of DTC. Under the premise of not changing the essence of the DTC algorithm, the torque ripple will always exist, so the experimental effect must still be incomparable with the experimental effect of the FOC algorithm.

B. DYNAMIC EXPERIMENTAL STUDY

To investigate the difference in dynamic performance of the three methods, experiments were carried out under

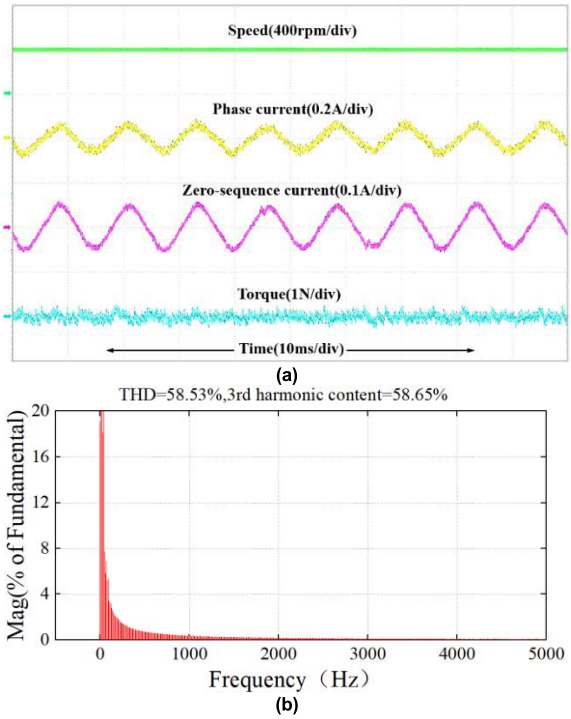

FIGURE 15. Experimental results of Method I at 400 r/min. (a) Speed, three-phase currents, ZSC and torque. (b) FFT analysis results.

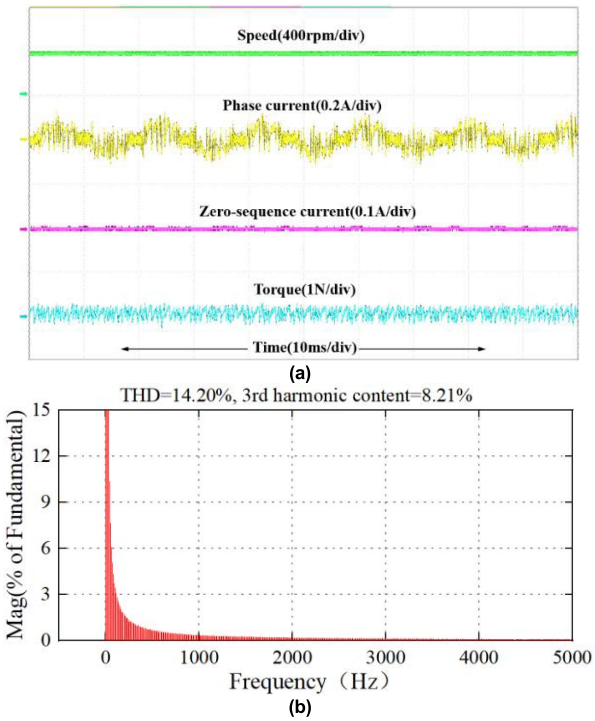

FIGURE 16. Experimental results of Method II at 400 r/min. (a) Speed, three-phase currents, ZSC and torque. (b) FFT analysis results.

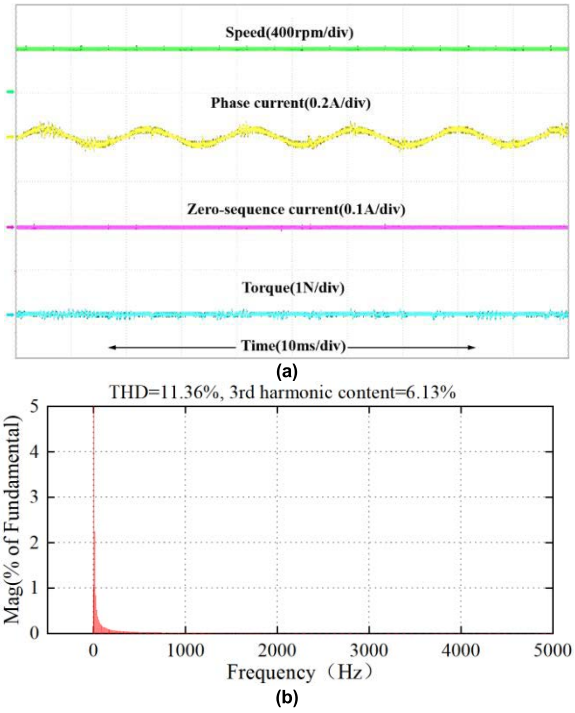

FIGURE 17. Experimental results of Method III at 400 r/min. (a) Speed, three-phase currents, ZSC and torque. (b) FFT analysis results.

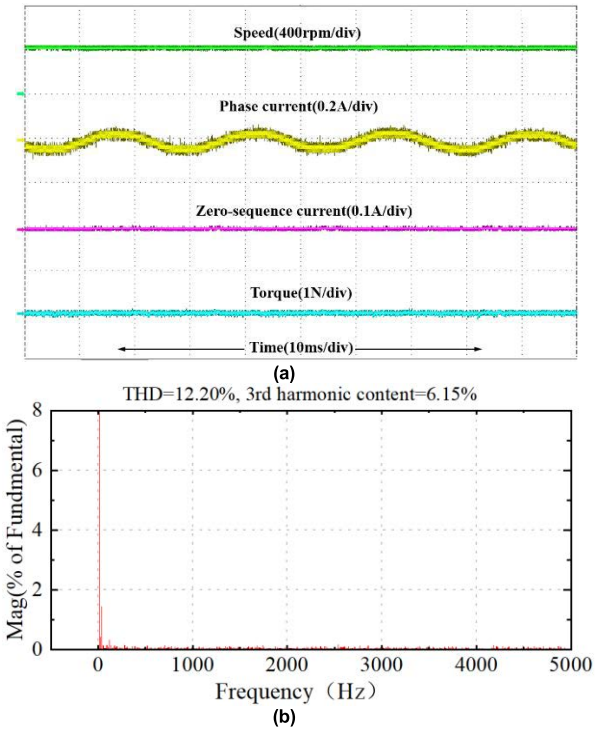

FIGURE 18. Experimental results of Method IV at 400 r/min. (a) Speed, three-phase currents, ZSC and torque. (b) FFT analysis results.

commutation and speed change, sudden loading and unloading conditions, and the results are shown in Figures 19 and 20. It can be seen from Figure 19 that the three methods have similar dynamic performance, and the reaction times of the three methods are the same during the sudden acceleration and sudden commutation of the motor. It shows that the proposed strategy improves the motor running condition without sacrificing the dynamic performance of the system, which is also the advantage of the proposed algorithm. When the speed reference changes, the phase current

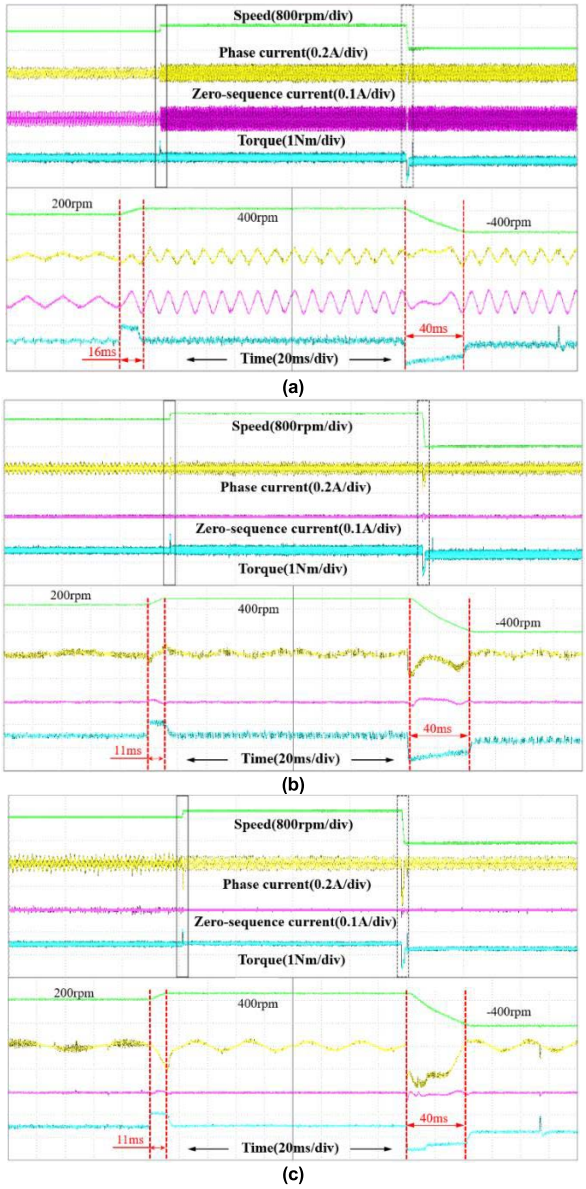

FIGURE 19. Dynamic performance comparison under speed changes condition. (a) Method I. (b) Method II. (c) Method III.

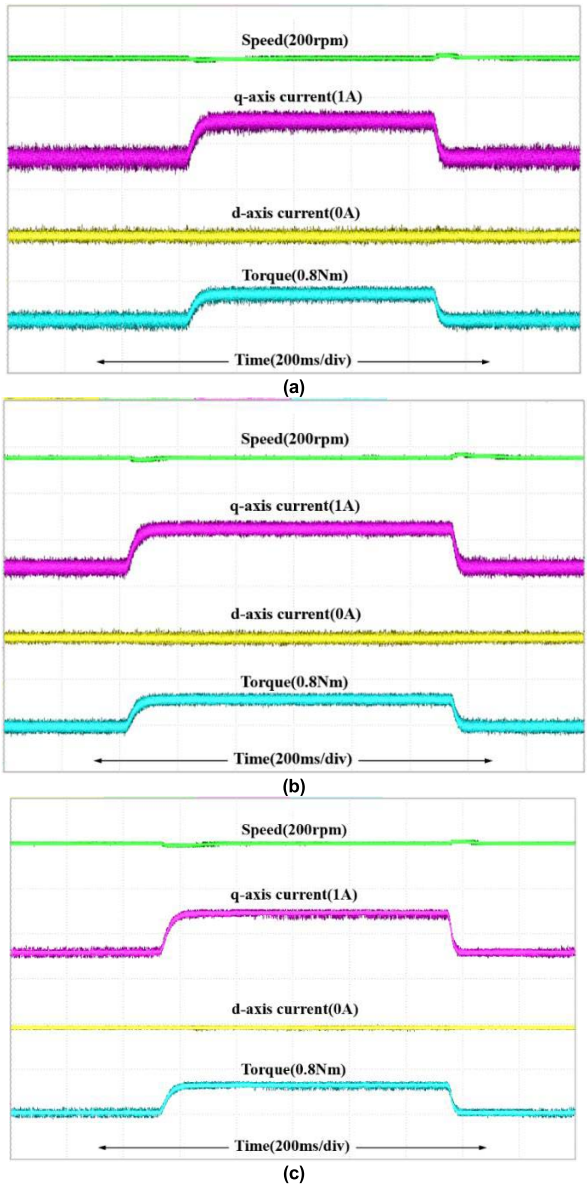

FIGURE 20. Dynamic performance comparison under loading/unloading condition. (a) Method I. (b) Method II. (c) Method III.

can respond quickly and complete the corresponding speed change work. In addition, there is no overshoot during rapid speed changes. The ZSC changes slightly during the dynamic change of the motor, but becomes zero soon after the motor is stable. This is because in the dynamic process of the motor, in order to meet the requirements of fast response, a little ability to control the ZSC is sacrificed. It shows that although the algorithm proposed in this paper increases the complexity of the algorithm, it does not affect the fast dynamic response capability of DTC. Figure 20 shows the noise immunity performance of the three methods under variable load conditions. The q-axis current and torque maintain this dynamic consistency, and can be quickly adjusted according to the magnitude of the load torque. At the same time, the speed will fluctuate slightly in the case of load disturbance, but it can recover quickly. The dynamic differences of the three methods are mainly reflected in the current and torque. Method III can maintain a fast dynamic response, while having better current and smaller torque ripple. These results demonstrate the good dynamic performance of the proposed method.

VI. CONCLUSION

This paper proposes a FLTH DTC, which is applied to the OEW-PMSM system of common DC bus. For the proposed strategy, the ZSC generated by the dual-inverter system and the common DC bus is calculated online, and the zero vector is applied to modulate to suppress the ZSC. At the same time, using the advantages of a large number of switching states owned by OEW-PMSM, a suitable voltage vector is selected, and a FLTH is used to reduce the torque ripple of the DTC system. Through comparative analysis, the optimal

width ratio of the two hysteresis loops is determined, and the goal of reducing the torque ripple of the system is achieved. The steady-state performance and dynamic performance of the proposed strategy are compared and analyzed. The results show that the performance of the proposed method is significantly better than the traditional DTC with ZSC and DTC with ZSC suppression. The proposed method suppresses the ZSC and reduces the torque ripple, while retaining the excellent dynamic response ability of the DTC algorithm, which provides some references and ideas for the application of electric vehicles.

REFERENCES

[1] S. Pramanick, M. Boby, N. A. Azeez, K. Gopakumar, and S. S. Williamson, "A three-level dodecagonal space vector-based harmonic suppression scheme for open-end winding IM drives with single-DC supply," *IEEE Trans. Ind. Electron.*, vol. 63, no. 11, pp. 7226–7233, Nov. 2016, doi: 10.1109/TIE.2016.2538205.

[2] X. Zhang, K. Wang, W. Zhang, Y. Wang, P. Wang, and D. Gao, "Dual delay-compensation-based model predictive control for the semi-controlled open-winding PMSM system," *IEEE Access*, vol. 7, pp. 69947–69959, 2019, doi: 10.1109/ACCESS.2019.2918445.

[3] X. Zhou, S. Li, M. Lu, F. Zeng, M. Zhu, and Y. Yu, "New fault tolerance method for open-phase PMSM," *IEEE Access*, vol. 7, pp. 146416–146427, 2019, doi: 10.1109/ACCESS.2019.2946183.

[4] X. Zhang and K. Wang, "Current prediction based zero sequence current suppression strategy for the semicontrolled open-winding PMSM generation system with a common DC bus," *IEEE Trans. Ind. Electron.*, vol. 65, no. 8, pp. 6066–6076, Aug. 2018, doi: 10.1109/TIE.2017.2784353.

[5] R. E. K. Meesala, V. P. K. Kunisetti, and V. K. Thippiripati, "Enhanced predictive torque control for open end winding induction motor drive without weighting factor assignment," *IEEE Trans. Power Electron.*, vol. 34, no. 1, pp. 503–513, Jan. 2019, doi: 10.1109/TPEL.2018.2812760.

[6] H. Zhan, Z. Q. Zhu, M. Odavic, and Y. Li, "A novel zero-sequence model-based sensorless method for open-winding PMSM with common DC bus," *IEEE Trans. Ind. Electron.*, vol. 63, no. 11, pp. 6777–6789, Nov. 2016, doi: 10.1109/TIE.2016.2585465.

[7] C. Liu and J. Shang, "Three-dimension space vector based finite control set method for OW-PMSM with zero-sequence current suppression and switching frequency reduction," *IEEE Trans. Power Electron.*, vol. 36, no. 12, pp. 14074–14086, Dec. 2021, doi: 10.1109/TPEL.2021.3087015.

[8] H. Zhan, Z. Q. Zhu, and M. Odavic, "Analysis and suppression of zero sequence circulating current in open winding PMSM drives with common DC bus," *IEEE Trans. Ind. Appl.*, vol. 53, no. 4, pp. 3609–3620, Jul./Aug. 2017, doi: 10.1109/TIA.2017.2679678.

[9] M. R. Baiju, K. K. Mohapatra, R. S. Kanchan, and K. Gopakumar, "A dual two-level inverter scheme with common mode voltage elimination for an induction motor drive," *IEEE Trans. Power Electron.*, vol. 19, no. 3, pp. 794–805, May 2004, doi: 10.1109/TPEL.2004.826514.

[10] X. Lin, W. Huang, W. Jiang, Y. Zhao, D. Dong, and X. Wu, "Direct torque control for three-phase open-end winding PMSM with common DC bus based on duty ratio modulation," *IEEE Trans. Power Electron.*, vol. 35, no. 4, pp. 4216–4232, Apr. 2020, doi: 10.1109/TPEL.2019.2935295.

[11] V. T. Somasekhar, S. Srinivas, and K. K. Kumar, "Effect of zero-vector placement in a dual-inverter fed open-end winding induction-motor drive with a decoupled space-vector PWM strategy," *IEEE Trans. Ind. Electron.*, vol. 55, no. 6, pp. 2497–2505, Jun. 2008, doi: 10.1109/TIE.2008.918644.

[12] H. Kubo, Y. Yamamoto, T. Kondo, K. Rajashekara, and B. Zhu, "Zero-sequence current suppression for open-end winding induction motor drive with resonant controller," in *Proc. IEEE Appl. Power Electron. Conf. Expo. (APEC)*, Mar. 2016, pp. 2788–2793, doi: 10.1109/APEC.2016.7468259.

[13] Y. Zhou and H. Nian, "Zero-sequence current suppression strategy of open-winding PMSG system with common DC bus based on zero vector redistribution," *IEEE Trans. Ind. Electron.*, vol. 62, no. 6, pp. 3399–3408, Jun. 2015, doi: 10.1109/TIE.2014.2366715.

[14] X. Yuan, S. Zhang, C. Zhang, M. Degano, G. Buticchi, and A. Galassini, "Improved finite-state model predictive current control with zero-sequence current suppression for OEW-SPMSM drives," *IEEE Trans. Power Electron.*, vol. 35, no. 5, pp. 4996–5006, May 2020, doi: 10.1109/TPEL.2019.2942156.

[15] X. Wang, Z. Wang, Z. Xu, M. Cheng, and Y. Hu, "Optimization of torque tracking performance for direct-torque-controlled PMSM drives with composite torque regulator," *IEEE Trans. Ind. Electron.*, vol. 67, no. 12, pp. 10095–10108, Dec. 2020, doi: 10.1109/TIE.2019.2962451.

[16] C. Xia, S. Wang, Z. Wang, and T. Shi, "Direct torque control for VSI–PMSMs using four-dimensional switching-table," *IEEE Trans. Power Electron.*, vol. 31, no. 8, pp. 5774–5785, Aug. 2016, doi: 10.1109/TPEL.2015.2498207.

[17] S. Wang, C. Li, C. Che, and D. Xu, "Direct torque control for 2L-VSI PMSM using switching instant table," *IEEE Trans. Ind. Electron.*, vol. 65, no. 12, pp. 9410–9420, Dec. 2018, doi: 10.1109/TIE.2018.2815995.

[18] R. Kumar and S. Das, "Sensorless DTC-SVM strategy for doubly-fed induction machine drive using model reference adaptive system," in *Proc. 14th IEEE India Council Int. Conf. (INDICON)*, Dec. 2017, pp. 1–6, doi: 10.1109/INDICON.2017.8487924.

[19] K. Tounsi, A. Djahbar, and S. Barkat, "DTC-SVM of five-phase permanent magnet synchronous motor drive," in *Proc. 8th Int. Conf. Modeling, Identificat. Control (ICMIC)*, Nov. 2016, pp. 103–108, doi: 10.1109/ICMIC.2016.7804281.

[20] D. Wang, T. Yuan, Z. Liu, Y. Li, X. Wang, W. Tian, S. Miao, and J. Liu, "Reduction of torque and flux ripples for robot motion control system based on SVM-DTC," in *Proc. 37th Chin. Control Conf. (CCC)*, Jul. 2018, pp. 5572–5576, doi: 10.23919/ChiCC.2018.8483131.

[21] A. Berzoy, O. Mohammed, and J. Rengifo, "Fuzzy predictive DTC of induction machines with reduced torque ripple and high-performance operation," *IEEE Trans. Power Electron.*, vol. 33, no. 3, pp. 2580–2587, Mar. 2018, doi: 10.1109/TPEL.2017.2690405.

[22] Y. Li, Y. Qu, X. Meng, H. Shi, and S. Jiao, "Voltage vector selection strategy of the DTC for SPMSM based on predictive control," in *Proc. 20th Int. Conf. Electr. Mach. Syst. (ICEMS)*, Aug. 2017, pp. 1–4, doi: 10.1109/ICEMS.2017.8056461.

[23] Y. Zhou and G. Chen, "Predictive DTC strategy with fault-tolerant function for six-phase and three-phase PMSM series-connected drive system," *IEEE Trans. Ind. Electron.*, vol. 65, no. 11, pp. 9101–9112, Nov. 2018, doi: 10.1109/TIE.2017.2786236.

YULEI YANG received the master's degree in electrical engineering from the Harbin Institute of Technology, in 2021, where he is currently pursuing the Ph.D. degree in electrical engineering.

His research interests include permanent magnet machines and drives.

QIAN WANG (Member, IEEE) received the Ph.D. degree in electrical engineering from the Harbin Institute of Technology, Harbin, China, in 2011.

Since 2011, he has been with the Institute of Specials Motors and Control, Harbin Institute of Technology, where he is currently an Associate Professor. His research interests include novel permanent magnet machines and drives, linear machines, and special electromagnetic actuation systems.

JING SHANG received the B.S., M.S., and Ph.D. degrees in electric engineering from the Harbin Institute of Technology, Harbin, China, in 1990, 1993, and 2004, respectively.

Since 2005, she has been a Professor with the Department of Electric Engineering, Harbin Institute of Technology. Her current research interests include permanent magnet motor design and drive, robotics, and resolver.